Environmental Science Advances

ROYAL SOCIETY OF CHEMISTRY

PAPER

View Article Online
View Journal | View Issue

Cite this: *Environ. Sci.: Adv.*, 2024, **3**, 819

Mineral formation explains the high retention efficiency of dissolved reactive phosphorus in a residential stormwater pond†

Mahyar Shafii, *[ab] Stephanie Slowinski, [ab] Md Abdus Sabur, [abc] Alina Arvisais,[ab] Yubraj Bhusal, [ab] William Withers,[d] Konrad J. Krogstad,[ab] Chris T. Parsons [ae] and Philippe Van Cappellen [ab]

Stormwater ponds (SWPs) alter the export of the macronutrient phosphorus (P) from urban landscapes, hence impacting the trophic state and water quality of downstream aquatic environments. Despite an increasing number of studies reporting P load reduction by SWPs, the mechanisms responsible for P retention remain unclear. We analyzed P chemical speciation and fluxes in the inflow and outflow of a SWP in the Toronto metropolitan area. In addition, we collected sediment cores to determine under what forms P accumulates in the SWP. The resulting P mass balance for the SWP yielded an average annual retention of 62% for total P (TP). Retention efficiencies varied significantly among the various TP fractions, however: 53% for particulate P (PP), 67% for total dissolved P (TDP), 66% for dissolved unreactive P (DUP), and >80% for dissolved reactive P (DRP), with DRP representing the most bioavailable TP fraction. Sequential chemical extractions performed on the sediment cores indicate that, with increasing sediment depth, the concentration of mineral-bound P increases while that of organic P decreases. We therefore attribute the efficient retention of DRP to biosynthesis of P-containing organic compounds followed by their post-depositional degradation and sequestration of the released phosphate ions by *in situ* precipitation of inorganic phases, primarily calcium (Ca) minerals. The conditions in the SWP are favorable to the formation of common Ca minerals, such as hydroxyapatite and calcite, including near-neutral to moderately alkaline pH values and high dissolved Ca^{2+} concentrations. In areas where urban runoff does not meet these conditions, interventions that stimulate P-containing mineral formation in SWPs may help reduce the export of DRP, hence, protecting receiving water bodies from eutrophication.

Received 8th September 2023
Accepted 13th March 2024

DOI: 10.1039/d3va00267e

rsc.li/esadvances

Environmental significance

Our manuscript presents the results of an extensive study on phosphorus (P) in a stormwater pond (SWP) located in Ontario, Canada. Although SWPs are usually assumed to act as a net sink of P in urban landscapes, significant variability in P retention by SWPs has been reported in the literature. In our study, we investigated the extent to which geochemical processes affecting P may help explain the variable P retention performance of SWPs. The key finding from our research is that dissolved reactive P (DRP) is largely retained by the SWP. We attribute this to the co-precipitation of P with calcium minerals in the sediments accumulating in the SWP. The immobilization of DRP (as a reactive P form) and its conversion to calcium-bound P (Ca–P as a stable P form) is a novel mechanism for reducing DRP in urban stormwater runoff. This is particularly important given that DRP is the most bioavailable form of P and, hence, the primary driver of algal blooms in P-limited freshwater ecosystems such as lakes and streams. From a water quality management perspective, it means that interventions that are able to induce Ca–P formation in SWPs may offer a management practice to reduce the risks of eutrophication of receiving freshwater bodies.The outcomes of our study advance the mechanistic understanding of P dynamics in urban SWPs, which, in turn, can inform strategies to use these systems as a means to protect downstream aquatic environments against excessive nutrient enrichment. Chemical processes enabling the retention of P are generally ignored when designing SWPs and other green stormwater infrastructure. Thus, our work should be of interest to both academic researchers and practitioners. The mechanistic and quantitative information derived from integrated approaches such as the one presented in our study can inform novel mitigation strategies in urban stormwater management.

[a]*Department of Earth and Environmental Sciences, University of Waterloo, Waterloo, Ontario, Canada. E-mail: mshafiih@uwaterloo.ca*

[b]*Water Institute, University of Waterloo, Waterloo, Ontario, Canada*

[c]*Department of Chemistry, Jahangirnagar University, Dhaka, Bangladesh*

[d]*City of Richmond Hill, Richmond Hill, Ontario, Canada*

[e]*Watershed Hydrology and Ecology Research Division, Environment and Climate Change Canada, Burlington, Ontario, Canada*

† Electronic supplementary information (ESI) available. See DOI: https://doi.org/10.1039/d3va00267e

1 Introduction

Global urban growth calls for the expansion and upgrading of stormwater management systems. Common reservoir-based systems, such as stormwater ponds (SWPs), were initially designed for peak flow attenuation and settling of suspended sediment.[1] They are now also considered as a potential practice

to protect water quality,[2] including by lowering the export of macronutrients, in particular phosphorus (P). Aquatic ecosystems receiving high P loads tend to exhibit excessive algal growth that, in turn, degrades water quality and threatens aquatic life.[3,4] Thus, controlling P loads from urban landscapes represents a key management strategy to lower the risk of worsening eutrophication in receiving water bodies.

Best management practices, such as reduced fertilizer applications and soil erosion control, have been successful in reducing P runoff from rural watersheds.[5] In urban catchments, characterized by ubiquitous impervious land cover, green infrastructure, such as SWPs and bioretention cells, provide a potential option to mitigate excess P export.[6,7] Phosphorus retention efficiencies of SWPs, however, are highly variable[8] and, in addition to pond size and morphology, also depend on the catchment's biophysical plus socio-economic characteristics and climatic conditions.[9]

Most P in urban runoff is bound to particulate matter.[10,11] Hence, the major pathway for P retention in SWPs is usually assumed to be the settling of P associated with incoming suspended matter and its accumulation in the bottom sediments.[12,13] Moreover, dissolved P uptake by shoreline and submerged vegetation, when accompanied by regular plant biomass removal, can act as a sink for dissolved P. Nonetheless, additional biogeochemical processes in SWPs affect the partitioning of P between dissolved and particulate chemical pools with variable reactivity and bioavailability.[14–16] For example, bottom sediments in SWPs can act as a source of dissolved phosphate because of the post-depositional degradation of labile particulate organic matter, not unlike the so-called process of internal P loading in wetlands and lakes.[12,15–17]

A key to unraveling the relative importance of physical and biogeochemical processes in regulating P retention in SWPs is to compare the fluxes and chemical speciation of P entering and leaving a SWP and those of the P retained in the sediments of the SWP. Here, we applied this approach to a SWP in the Toronto metropolitan area, Canada. Sequential chemical extractions performed on samples from sediment cores recorded the multi-year accumulation and transformations of P in the SWP's bottom sediments. These sediment data were combined with an entire year of data on discharge plus dissolved and particulate P concentrations in the SWP's inflow and outflow, supplemented with rainfall-runoff modeling to fill hydrologic data gaps and statistical models to quantify annual P in- and outflow loads. Together, the results enabled us to determine speciation-specific P mass balances and retention efficiencies and infer the underlying mechanisms.

2 Material and methods

2.1 Study site

The SWP (43°53′23.3″N, 79°24′10.0″W) is located in the City of Richmond Hill within the Greater Toronto Area, Ontario, Canada. It was built in 1998 and drains a 10.5 ha fully residential catchment consisting of single-family dwellings. The catchment's impervious land cover is around 50%. The pond discharges into the Rouge River, a tributary of Lake Ontario. The SWP's permanent pool storage capacity is 2055 m^3 and the active pool storage capacity is 2676 m^3, yielding a total storage capacity of 4786 m^3. Fig. 1 illustrates the layout of the different pond compartments. The SWP's open water surface area at the permanent level is 2255 m^2. A 1 m diameter inlet sewer directs the catchment runoff into a forebay, followed by the main basin. The pond's outlet consists of a 300 mm diameter sewer with a reverse slope pipe and an 80 mm diameter discharge orifice. This configuration hydraulically attenuates outflow discharge by temporarily storing excess stormwater in the SWP during rainfall and snowmelt events. The major littoral plants growing in and around the SWP are reed (genus: *Phragmites*) and cattail (genus: *Typha*).

2.2 Field data collection

2.2.1 Discharge and meteorological data. Teledyne ISCO 4150 area-velocity flowmeters were installed in the inlet and outlet sewers. Rating curves for both inlet and outlet were derived from semi-continuous (5 minutes) flow and water level data measured from October 2020 to March 2021. The flowmeters malfunctioned between March 26, 2021, and the end of 2020 water year (*i.e.*, September 2021). A simple rainfall-runoff model was used to bridge discharge data gaps based on water levels recorded in the SWP and weather (precipitation and temperature) data from the Oak Ridges station located 7.5 km away from the pond and operated by the Toronto and Region Conservation Authority or TRCA (see section 2.4.2 for details).

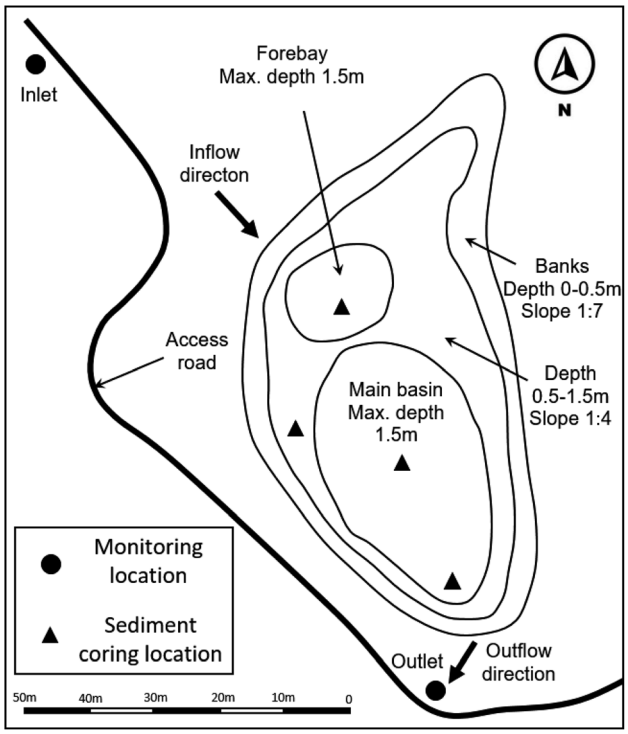

Fig. 1 Richmond Hill stormwater pond (SWP): view from above indicating the locations of the inlet and outlet storm sewer maintenance holes where sampling and flow equipment was installed, as well as the four sediment core sampling locations in the SWP.

2.2.2 Water and suspended sediment sampling. Over the monitoring period, stormwater samples were collected in the inlet and outlet sewers during a total of 14 rain and snowmelt events. The event characteristics and the corresponding average inflow P concentrations are given in Table 1. Between events there was no baseflow in the sewers. We used Teledyne ISCO automated samplers (model 6712), equipped with 24 sample bottles (each 1 L) and connected to level- and flowmeters, to collect water samples from the inlet and outlet sewers during each event. Before an event, the samplers were programmed to be triggered by a water level rise of 25 mm. The time interval was adjusted for the season and the anticipated event magnitude, intensity, and duration to capture all components of the hydrograph.[18] For each event, a subset of 6 ISCO bottles (out of 24) were selected: two at the start of the event (early flush water), two on the hydrograph's rising limb, and two on the falling limb. Samples (1 L) of the pond water column were also collected between rain events when we were onsite to retrieve the samples collected by the ISCO samplers. All pond water samples were taken from the surface of the water column at the same location within a meter of the pond bank close to the outlet.

The relatively low amounts of total suspended sediments obtained with the ISCO samplers did not allow individual P speciation analyses. We therefore collected a composite sample from the inlet during the November 11, 2020, event by combining the contents of the 24 ISCO bottles in volumes proportional to their corresponding flow discharges. The combined sample was transported to the lab and centrifuged at 2516 G for 15 minutes. Two other suspended sediment samples (1 from the inlet on December 15, 2021, and 1 from the outlet on December 13, 2021) were collected by deploying a newly acquired portable continuous flow centrifuge on-site (CFC Express, Scientific Methods Inc., Granger, IN) and operated at a rotational speed of 4472 G. The P speciation of the three suspended sediment were analyzed as described in section 2.3.4.

2.2.3 Sediment coring. Four sediment cores were collected with a Universal Corer (Aquatic Research Instruments, Hope, ID) on February 24, 2021, from the following locations (Fig. 1): (1) the sedimentation basin (hereafter called "forebay"), (2) the middle of the main basin ("mid-pond"), (3) near the outlet of the main basin ("near-outlet"), and (4) near the bank of the main basin along the vegetated shoreline ("bank"). The topmost 14, 6, and 4 cm of, respectively, the forebay, mid-pond, and near-outlet cores consisted of soft black sediment overlying the compacted grey sediment that corresponds to the original bottom of the SWP. Hence, the depth intervals of soft black sediment were assumed to record the depositional history at the coring sites since the SWP was last dredged in 2006. The topmost 4 cm of coarser sediment in the bank core were similarly assumed to represent the post-2006 sediment accumulation. The cores had an inner diameter of 6.8 cm and were sectioned into 1 cm intervals within 24 hours of collection. The sections were stored in Whirl Pak bags at −20 °C before freeze-drying. Each freeze-dried sediment sample was ground using a mortar and pestle and sieved to <125 μm using a stainless-steel sieve.

2.3 Analytical methods

All containers used for analyses or storing samples, including the polyethylene bottles in the ISCO samplers, were washed with a citric acid solution at 75 °C followed by rinsing with 18.2 MΩ cm^{-1} ultra-pure water. Within 72 hours of sample collection, 60 mL of a water sample was filtered into a polyethylene centrifuge tube through a 0.45 μm pore size nylon membrane syringe filter (VWR® Syringe Filters, VWR International), unless otherwise specified. Next, the filtrate was divided into two aliquots:

Table 1 Summary of inflow events showing dates of sampling, mean inflow concentrations of total phosphorus (TP), total dissolved phosphorus (TDP) and reactive dissolved phosphorus (DRP), and other event characteristics[a]

Date	Average inflow concentration (mg L^{-1})			Event duration (hours)	Average discharge (L s^{-1})	Maximum discharge (L s^{-1})	Integrated event volume (L)	Average precipitation (mm)	Average air temperature (°C)
	TP	TDP	DRP						
11-Nov-20	0.74	0.16	0.014	4	1.3	2.22	9328	0.3	11.3
15-Nov-20	0.34	0.14	—	17	3.5	20.8	165 891	12.5	8.4
25-Nov-20	0.04	0.02	0.019	31	5.7	13.3	225 206	8.7	3.8
30-Nov-20	0.09	0.01	0.007	12	5.3	15.2	191 988	12.1	3.2
11-Dec-20	0.21	0.03	0.020	8	12.6	23.5	135 747	7.2	5.6
24-Feb-21	0.17	0.08	0.059	U*	U*	U*	U*	U*	1.5
8-Mar-21	—		0.067	1	S**	S**	S**	0.3	0.7
11-Mar-21	0.2		0.095	11	0.6	0.7	10 333	1.6	11.1
26-Mar-21	0.17		0.047	17	19	69.1	1 094 997	31.6	7.5
8-Jul-21	0.09		0.058	16	35.2	77.6	1 522 552	36.1	18.5
13-Jul-21	0.33	0.11	0.054	10	23.7	50.6	767 149	16.8	23.2
29-Jul-21	0.08	0.03	0.024	10	8.1	17.2	263 924	8.6	18.1
10-Aug-21	0.03	0.02	0.016	1	S**	S**	S**	0.1	24.8
8-Sep-21	0.09	0.02	0.013	15	20.1	37.5	1 087 379	27.2	20.6
14-Sep-21	0.21	0.05	0.044	8	31.5	60.1	908 224	17.7	18
21-Sep-21	0.16	0.04	0.030	21	29.5	55.3	2 017 595	47.7	20.8

[a] U*: unknown or snowmelt event, S**: small event or no model runoff.

(i) 10 mL (unacidified) for dissolved reactive P (DRP) and dissolved inorganic carbon (DIC) analyses, and (ii) 10 mL acidified with ultra-pure nitric acid (final concentration 2% v/v) for ICP-OES analyses (Thermo Scientific iCAP 6300). Both unfiltered and filtered aliquots were stored at 4 °C prior to the analyses.

2.3.1 Inflow, outflow, and pond water: P speciation. The concentrations of three operationally defined P fractions, total P (TP), total dissolved P (TDP) and dissolved reactive P (DRP), were measured in the stormwater and pond water samples. Concentrations of DRP were measured with the molybdenum blue spectrophotometric method[19,20] (see ESI S5† for details). Concentrations of TDP were measured by ICP-OES on the acidified filtered aliquots (MDL: 0.4 μmol L^{-1}). For TP, the unfiltered sample was digested in an autoclave in acid persulfate solution[21] followed by ICP-OES analysis (MDL: 0.08 μmol L^{-1}). The concentrations of dissolved unreactive P (DUP) and particulate P (PP) were calculated by difference from the measured TP, TDP and DRP concentrations.[22] Note that the operational definition of DUP as the difference TDP – DRP means that DUP may contain dissolved organic compounds containing P, some of which may be enzymatically degradable.[23]

2.3.2 Additional water analyses. The following analyses were carried out on stormwater and pond water samples. Dissolved inorganic carbon (DIC) was determined on a TOC analyzer (Shimadzu; MDL: 0.046 mmol L^{-1}). Total dissolved concentrations of calcium (DCa) were determined by ICP-OES at the same time as TDP in the 0.45 μm-filtered water samples (MDL: 0.23 μmol L^{-1}). Additional water chemistry variables were used in mineral saturation index calculations (see section 2.4.1 and ESI section S2†). Values of pH were obtained in the lab within 72 hours of sample collection. Depth profiles of temperature and specific conductivity in the SWP water column were measured on February 24, 2021 (Winter) with an XR-620 profiler (RBR Ltd.) and on June 23, 2022 (Summer) with a YSI EXO2 Multiparameter Water Quality Sonde (Xylem Inc.). The winter profile was collected when the SWP was ice-covered.

2.3.3 Sediment geochemistry. Total organic carbon (TOC) and total nitrogen (TN) concentrations of the sediment samples were analyzed by combustion analysis at 550 °C on a vario EL cube (Elementar Analysensysteme GmbH). Samples were prepared by weighing approximately 30 mg of (freeze-dried, ground and sieved) sediment into tin wraps. The MDL was 1 wt% for both TOC and TN. Values of TN fell below the MDL in all the sediment core samples. Total P (TP) concentrations were obtained according to Aspila *et al.*[24] by adding 1 mL of 100% w/v magnesium nitrate to 0.1 g (0.1 mg precision) of freeze-dried sediment and then ashing at 550 °C in a muffle furnace for 2 hours. Next, the ashed sediment was resuspended in 10 mL of 1 M HCl and shaken for 16 hours before filtering through a 0.45 μm pore size nylon membrane filter. The filtrate was 10-times diluted with 2% nitric acid and analyzed by ICP-OES. The MDL was 0.05 μmol P g^{-1}. On 25% of the samples duplicate TP extractions were performed: the average percent difference between duplicates was 1.9%. The freeze-dried and ground sediment samples were also analyzed by X-ray diffraction (XRD) and scanning electron microscopy and electron dispersive spectroscopy (SEM-EDS) (see ESI S3† for details).

2.3.4 Sediment phosphorus speciation. A subset of the sediment core sections was analysed using the SEDEX sequential extraction method of Ruttenberg[25] with the additional step proposed by Baldwin[26] to extract P bound to humic substances. The method extracts six operationally defined P pools in the following sequence: (1) P_{Ex}: easily exchangeable and loosely-sorbed P (1 M $MgCl_2$), (2) P_{Hum}: humic-bound P (1 M $NaHCO_3$ at pH 7.6), (3) P_{Fe}: redox-labile P associated with Fe and Mn (hydr)oxides (1 M citrate-dithionite-bicarbonate, CDB, solution), (4) P_{Ca}: non-redox mineral Ca-bound P (1 M acetate at pH 4), (5) P_{Inorg}: detrital apatite and other inorganic P (1 M HCl), and (6) P_{Org}: organic P (1 M HCl following ashing at 550 °C). The first three extractions (P_{Ex}, P_{Hum} and P_{Fe}) release the most reactive particulate P forms and are therefore most likely to act as sources of dissolved phosphate, while the next two P pools (P_{Ca}, P_{Inorg}) are known to be much more stable.[15,27] The last pool, P_{Org}, may contain both relatively reactive and recalcitrant organic compounds. Without the added 1 M $NaHCO_3$ step, the humic-bound P pool would be released together with the redox-labile P pool during the CDB extraction. Further details on the performance of the SEDEX method with the added 1 M $NaHCO_3$ step are presented in earlier work.[15,27]

The sequential extractions were performed on nine sediment core sections along with three stormwater suspended sediment samples (section 2.2.2). The sediment depth intervals analyzed were: four from the forebay core (0–1, 5–6, 12–13 and 21–22 cm), one from the bank core (3–4 cm), two from the mid-pond core (0–1 and 3–4 cm), and two from the near-outlet core (0–1 and 3–4 cm).The sequential extractions were conducted on 0.1 g sediment using the manifold system developed by Ruttenberg *et al.*[28] Each sample was extracted in duplicate. Each extract was diluted 1 : 10 in a 2% nitric acid matrix and the total dissolved P concentrations of the diluted extracts were measured by ICP-OES.

Calibration curves for each sequential extraction step were obtained using matrix-matched standards. The sum of the SEDEX fractions varied by less than 8% among duplicate extractions. Duplicate extractions of certified EU Community Bureau of Reference (BCR) Reference Material No. 684 "River sediment (extractable phosphorous)" were also performed for each batch of 8 core samples. The SEDEX TP (*i.e.*, the sum of all the SEDEX fractions) in the BCR reference material were within 5% of the certified TP value. Hereafter, the relative concentrations of the extracted P pools are expressed as fractions of SEDEX TP rather than the single point extracted TP from the Aspila *et al.* method[24] (section 2.3.3). The SEDEX TP was within 10% of the single point extraction TP, albeit usually slightly lower. The TP concentrations obtained with the single point extraction on the BCR certified reference material were within 6% of the certified TP value.

2.4 SWP P budget: modeling steps

2.4.1 Mineral saturation index calculations. Saturation indexes (SI) of various phosphate minerals plus calcite were calculated based on the measured chemical composition and temperature of the pond water samples. They were computed with the PHREEQC Interactive 3.3.7 program using the thermodynamic data in the PHREEQC database,[29] except for the

equilibrium constants of the dissolution reactions of calcium phosphate phases that were taken from Dorozhkin[30] and are listed in Table S1.† We imposed the water temperature data recorded in the outlet sewer with a HOBO Pendant MX Water Temperature Data Logger. Gaps in the dataset were filled using the available local air temperature records and season-specific regressions between measured air and water temperatures.

2.4.2 Filling discharge data gaps. Catchment rainfall-runoff modeling similar to previous work on urban catchments[31,32] was used to fill data gaps in measured discharge at the pond inlet (details in section S1 of the ESI†). The model was calibrated with observations for all events with complete flow records between October 2020 and December 2021. Events were identified as follows: (1) the total cumulative discharge of the event had to be at least 100 L, and (2) there was no flow within six hours before and after the event. Hourly time steps with discharge less than 1 L s^{-1} were considered as no flow. Once all events were identified, the goodness-of-fit between simulated and observed cumulative flow was evaluated for all the events with the Nash–Sutcliffe Efficiency (NSE) metric.[33] After setting lower and upper bounds for the model parameters, 50 000 Monte Carlo simulations were run assuming uniform probability distributions over the assigned parameter ranges. The simulation with the highest NSE (*i.e.*, closest to 1) was selected as the calibrated model. The latter was then used to produce uninterrupted hourly discharge time series for the catchment outlet (*i.e.*, the pond inlet).

For the pond outlet, a polynomial relationship between discharge and pond water level was developed. Outflow occurs when the water level rises to that of the outlet sewer's orifice located at elevation 213.45 m. A time series of the difference between pond water level and outlet orifice level was generated using the daily pond level data provided by the City of Richmond Hill. Together with the available measured outflow discharge data, the following polynomial relationship between flow and differential level was then derived:

$$Q_o = 34.9L_d^3 - 2.08L_d^2 - 0.035L_d + 0.007 \quad (1)$$

where Q_o is the outflow discharge (in m^3 s^{-1}) and L_d is the level difference (in m) $L_d = \max(L_p - 213.45,0)$ with L_p being the measured pond water level (in m). Level differences L_d greater than 0.25 m were set equal to 0.25, assuming that Q_o reaches its maximum value at that level. The value of 0.25 m was based on the calibration of the flow model by maximizing the fit of simulated and observed time series of discharge at the outlet. Eqn (1) was used to fill data gaps in the measured outflow discharge (Q_o).

2.4.3 Statistical modeling of P loads. Multiple linear regression (MLR) models were developed in Matlab to generate time series of the instantaneous loadings of the different P pools based on the following explanatory variables: (1) the instantaneous log-transformed flow (Q_i) at the time of collection of the water sample i, (2) the sampling month (M_i), (3) the cumulative seven-day precipitation depth prior to sampling (P_i), (4) the average temperature during the 14 days prior to sampling (T_i), and (5) the number of dry days during the 14 days prior to sampling (DD_i). Variables 3, 4, and 5 were extracted directly from meteorological data (section 2.2.1). The explanatory variables were chosen because of the ample availability of flow and meteorological data, and because preliminary analyses showed that other flow and precipitation metrics closely correlated with the selected variables without yielding better model outcomes. Air temperature was included as a climate metric in the list of potential explanatory variables for P export. Note that, because we used stepwise MLR methods, any explanatory variable that did not show a significant effect on the dependent variable was automatically discarded.

The MLR models estimated log-transformed instantaneous loadings ($L_{n\times1}$) for both inlet and outlet according to the following matrix formulation:

$$L_{n\times1} = X_{n\times(k+1)}\beta_{(k+1)\times1} + \varepsilon_{n\times1} \quad (2)$$

where n is the number of datapoints, k is the number of explanatory variables, X is the matrix of (independent) explanatory variables, β is the vector of regression coefficients, and ε is the random error component that accounts for the difference between the observed and fitted linear relationship. The number of columns in X is k+1 because there are k explanatory variables plus the intercept. Note that the MLR approach allowed for multiplicative (*e.g.*, Q_iM_i, Q_iP_i, *etc.*) and quadratic (*e.g.*, Q_i^2, M_i^2, *etc.*) terms. Therefore, k could in principle be greater than five. We ran MLR models in 100 trials where, in each trial, a subset of randomly chosen independent variables (X) was log-transformed while the rest of the variables were not transformed. The corresponding modeling trials produced different outcomes (*i.e.*, load estimates) that were used to delineate ranges in annual P loadings and retention efficiencies.

The goodness-of-fit (*i.e.*, NSE) of the simulated loads generated by the MLR models were assessed by comparison with the observed instantaneous loads (mg) estimated by multiplying the measured flow rates (L s^{-1}) by the length of time between consecutive flow records (s) and the measured concentrations (mg L^{-1}). We also checked the residuals' normality with the Shapiro–Wilk (SW) test[34] and homoscedasticity with the Breusch–Pagan (BP) test.[35] For each MLR model, we tested several scenarios where different subsets of explanatory variables were log-transformed until we achieved a satisfactory model performance (with respect to NSE) with normally distributed and homoscedastic residuals.

To account for uncertainties associated with the MLR-predicted P loads, a probabilistic approach to generate MLR model outcomes was used. Specifically, 100 realizations of the distributions of the MLR coefficients were sampled and used to simulate 100 P loading time series. Statistically, a realization from the distribution of coefficient β can be obtained using $\hat{\beta}$ + $T_{n-p}E_\beta$ where $\hat{\beta}$ is the MLR estimate for the coefficient, T_d is a realization from t distribution with d degrees of freedom, n is the number of observations, p is the number of variables (*i.e.*, number of explanatory variables plus one), and E_β is the standard error of the MLR estimate for coefficient β. The MLR models were calibrated against P data collected in 2020–2021. Load simulations for all time steps between October 1, 2020,

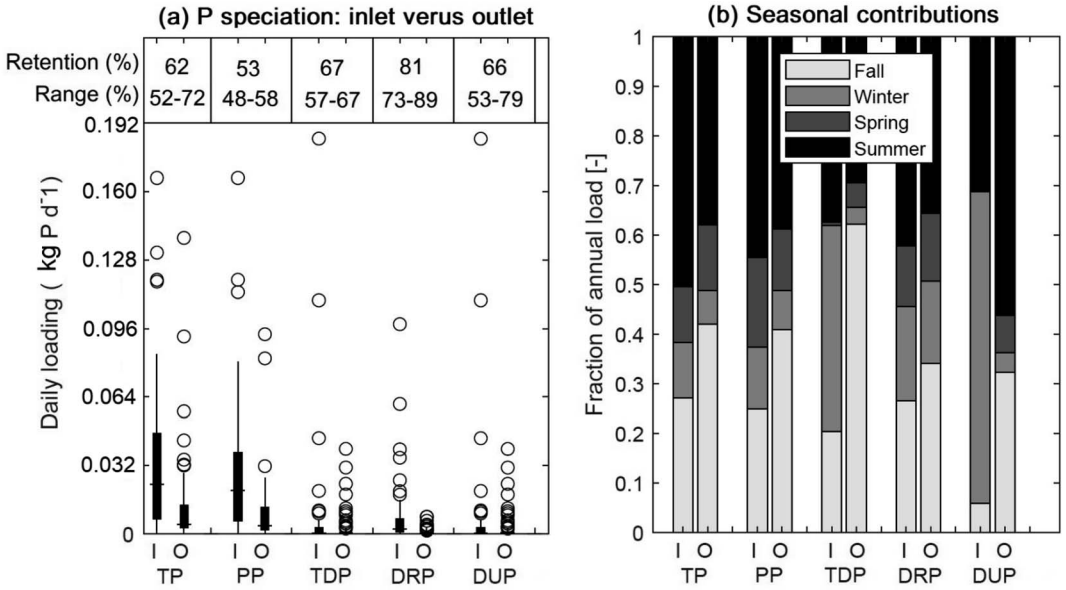

Fig. 2 Phosphorus (P) speciation in the SWP inlet (I) and outlet (O) (a), and seasonal contributions of the different P pools to the annual loadings (b). In (b), the load predictions are based on the MLR results between October 2020 and September 2021 for pond inlet (I) and outlet (O). Note that (i) circles and solid boxes in (a) correspond to the outliers and inter-quartile ranges, respectively, (ii) numbers on top of left panel show annual retentions and the corresponding ranges, and (iii) seasons are defined as September–November (fall), December–February (winter), March–May (spring), and June–August (summer).

and September 30, 2021, were time-integrated to estimate the annual loads of TP and those of the individual P fractions P entering and leaving the SWP.

2.4.4 Phosphorus mass balance modeling and retention efficiencies. The following mean annual TP fluxes were estimated: (1) the inlet flux (F_{IN}), (2) the atmospheric deposition flux (F_A), (3) the retained flux (F_B), and (4) the outlet flux (F_{OUT}). Atmospheric TP deposition rates reported for southern Ontario range from 0.09 to 0.58 kg ha^{-1} per year.[36,37] This range was multiplied by the SWP's surface area to determine the range of F_A. The difference between influx and outflux was considered as the retained flux F_B. The hourly time series generated for flow and TP concentrations at the SWP's inlet and outlet (section 2.4.3) were used to calculate F_{IN} and F_{OUT} for the entire hydrological year (October 1, 2020, to September 30, 2021). Seasonal and annual retention efficiencies of TP and those of the individual TP fractions (section 2.3.1) were calculated as the corresponding difference between inflow flux and outflow flux, divided by the inflow flux.

3 Results

3.1 Discharge and P loads

The calibrated rainfall-runoff model for the pond inflow had an NSE value of 0.65 for the event-based cumulative flow as the predicted variable. The MLR modeling further yielded less frequent outflow events than stormwater inflow events, especially during the summer. As expected, peak outflow discharges were attenuated relative to those observed for the inflow. Fig. S1 in ESI† provides the cumulative distribution function of inlet discharge in the calibration time frame, as well as the precipitation and discharge time series (inlet and outlet) for the simulation period outside of the calibration time window. Integrated over the entire hydrological year 2020–2021, the total annual inflow was around 20 000 m^3. Given the permanent storage of the SWP of 2055 m^3 (section 2.1), this translates into a nominal water residence time of 9.7 days.

The model-predicted ranges of the daily loads of the different P pools for both inlet and outlet are shown in Fig. 2a. The generally lower values for the outflow TP loads than the inflow TP loads reflect P retention in the SWP. Mean annual retention efficiencies and their ranges (based on 100 MLR model trials) are given (in %) at the top of Fig. 2a. On average, the best retention was observed for DRP (81%), followed by TDP (67%). In addition to the annual trends in Fig. 2a, seasonal variations of the seasonal P speciation in inflow and outflow are illustrated in Fig. 2b. As can be seen, with the exception of inflow TDP and DUP, most of the annual loadings into and out of the SWP occurred during summer and fall. These seasons also experienced the highest amounts of flow (Fig. S2†). For TDP and DUP, the largest contributions to the respective annual inflows were observed during winter. Most DUP export from the SWP occurred during summer, however.

3.2 Phosphorus mass balance

The SWP's mean annual TP balance and associated P speciation results are summarized in Fig. 3. Atmospheric TP deposition accounted for about 0.06 kg per year (F_A range: 0.02–0.12 kg per year). The flow-weighted mean TP inlet and outlet loads were estimated at 2.5 kg per year (F_{IN} range: 2.3–2.7 kg per year) and 1.3 kg per year (F_{OUT} range: 1.1–1.5 kg per year), resulting in retained flux (F_B) of 1.3 kg per year with a range of 1.1–1.6 kg per year. The same information provided in Fig. 3 is also shown in

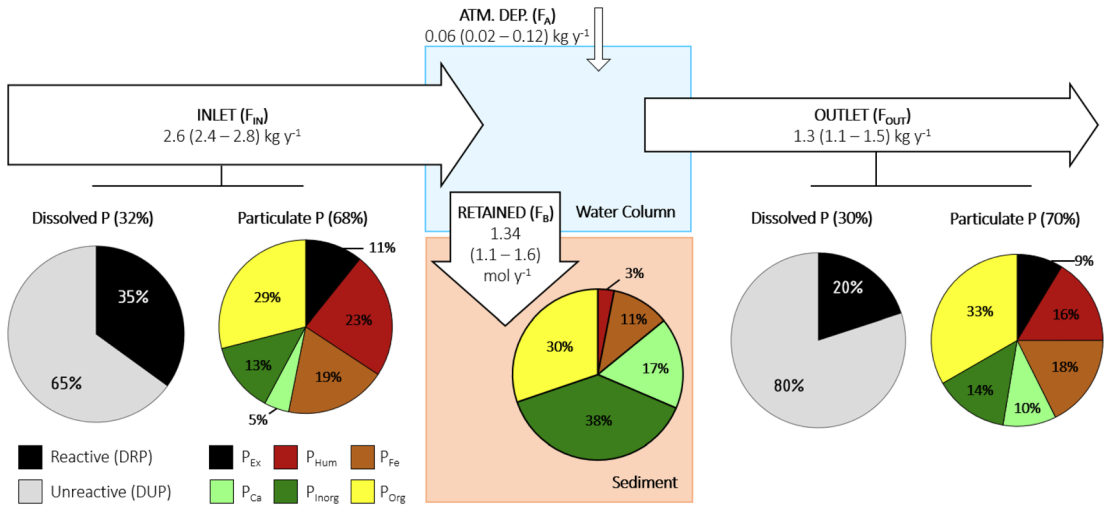

Fig. 3 Annual phosphorus mass balance of the Richmond Hill SWP showing the TP mass fluxes into and out of the pond water column *via* the inlet stormwater flow plus atmospheric deposition, the outlet stormwater flow, and burial in the sediments. The diagram also shows the average P speciation in the dissolved P pools (DUP and DRP) and the particulate P pools (P_{Ex}, P_{Hum}, P_{Fe}, P_{Org}, P_{Ca} and P_{Inorg}) determined based on the sequential chemical extraction results. Note that DUP is defined as TDP – DRP and may contain some potentially degradable dissolved organic P compounds.

the ESI material (Fig. S3)† with units of mol per year. Note that the mean values reported above were determined based on averaging the outcome of 100 realizations of the MLR models with the 95% confidence intervals estimated assuming normal distributions.

3.3 Sediment geochemistry and P speciation

The TP concentrations in the sediment cores ranged from 19.4 to 27 μmol g^{-1} with a mean of around 25 μmol g^{-1} (Fig. 4a). They showed little change (<10%) with depth below the sediment–water interface (SWI), apart from the bank core where the TP concentration dropped from about 24 μmol g^{-1} at the top to 19 μmol g^{-1} at the bottom of the core (*i.e.*, in the 5–6 cm depth interval). In contrast to TP, the TOC concentrations varied significantly among the cores and with depth in each core (Fig. 4b): they ranged from 1.1 to 7.9 mmol g^{-1} (1.3 to 9.5 wt%) with a mean of 3.8 mmol g^{-1} (4.6 wt%). Furthermore, the TOC concentrations systematically decreased with increasing depth below the SWI (average decrease of 30% between topmost and bottom samples across the 4 cores). The forebay sediment was the most enriched in TOC, the bank sediment the least. In addition, across the pond, the mean sediment TOC concentration decreased from the forebay to the mid-pond to the near-outlet core.

In terms of TP and TOC concentrations, the sediment composition in the SWP falls within the ranges reported for other urban open water bodies.[17,38,39] The XRD and SEM-EDS results further revealed the presence of pyrite (Table S2†) with a framboidal texture (Fig. S4†) in the forebay, main basin and near-outlet main basin cores. Calcite was abundantly present in the sediment, while siderite (ferrous iron carbonate) was also detected in all core samples (Table S2†).

In the forebay, mid-pond and near-outlet sediment cores, both the concentrations and the proportions of P_{Ex}, P_{Hum} and P_{Org} generally decreased with depth while the contributions of P_{Ca} and P_{Inorg} increased (Fig. 5), except for the relative contribution of P_{Inorg} in the mid-pond sediment core which showed no increase with depth. The concentration and proportion of P_{Fe} exhibited no discernible depth trends in the cores. Thus, overall, the most reactive P fractions (P_{Ex}, P_{Hum} and P_{Org}) were replaced by more stable P fractions (P_{Ca} and P_{Inorg}) with increasing depth. This was most evident in the longer forebay core: between the 3–4 cm depth interval and the 12–13 cm depth interval, the combined contributions of P_{Org}, P_{Hum} and P_{Ex} to TP decreased from 36% to 26% whereas the combined contributions of P_{Inorg} plus P_{Ca} increased from 48% to 56%.

A linear sediment accumulation rate of 2.4 cm per year was estimated for the forebay zone by dividing the total sediment depth by the years since pond was last dredged until when the cores were retrieved (*i.e.*, 2021). By combining the linear sedimentation rate with concentration differences between core sections, we obtained an average rate of 1 μmol g^{-1} per year at which the sum of the reactive P pools decreased with time (Fig. S5†). This rate was mirrored by that at which the sum of the stable P pools increased of 1.2 μmol g^{-1} per year. For a starting concentration of the combined reactive P pools of about 12 μmol g^{-1} (*i.e.*, the concentration in the shallower core section) this translates to a half-life of around 8 years. For the mid-pond and near-outlet cores, similar calculations of the transformations rates of the combined reactive P pools yielded 0.7 and 3.4 μmol g^{-1} per year, respectively, or half-lives of 14 and 4 years.

The TP concentrations of the inlet stormwater suspended sediment samples collected in Fall 2020 (75 μmol g^{-1}) and Winter 2021 (50 μmol g^{-1}) were higher than the average TP concentration of the sediment core samples (25 μmol g^{-1}). The proportions of the SEDEX P pools in Fall 2020 were, for the most part, comparable to those observed in the top-most sections of the forebay, mid-pond and near-outlet cores (compare Fig. 5 and 6). However, the Fall 2020 inlet suspended sediment

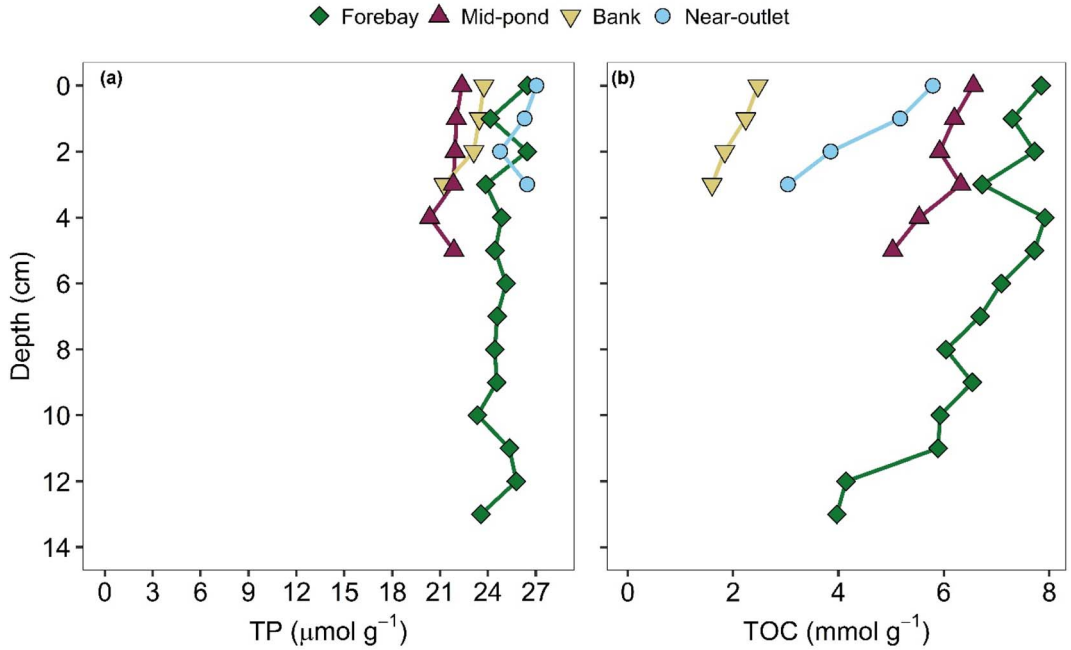

Fig. 4 Depth profiles of total phosphorus (TP) (a) and total organic carbon (TOC) (b) concentrations in the four sediment cores sampled from four different locations in the pond (forebay, bank, mid-pond and near-outlet, see Fig. 1). On the vertical axis, the origin (zero) corresponds to the sediment–water interface (SWI).

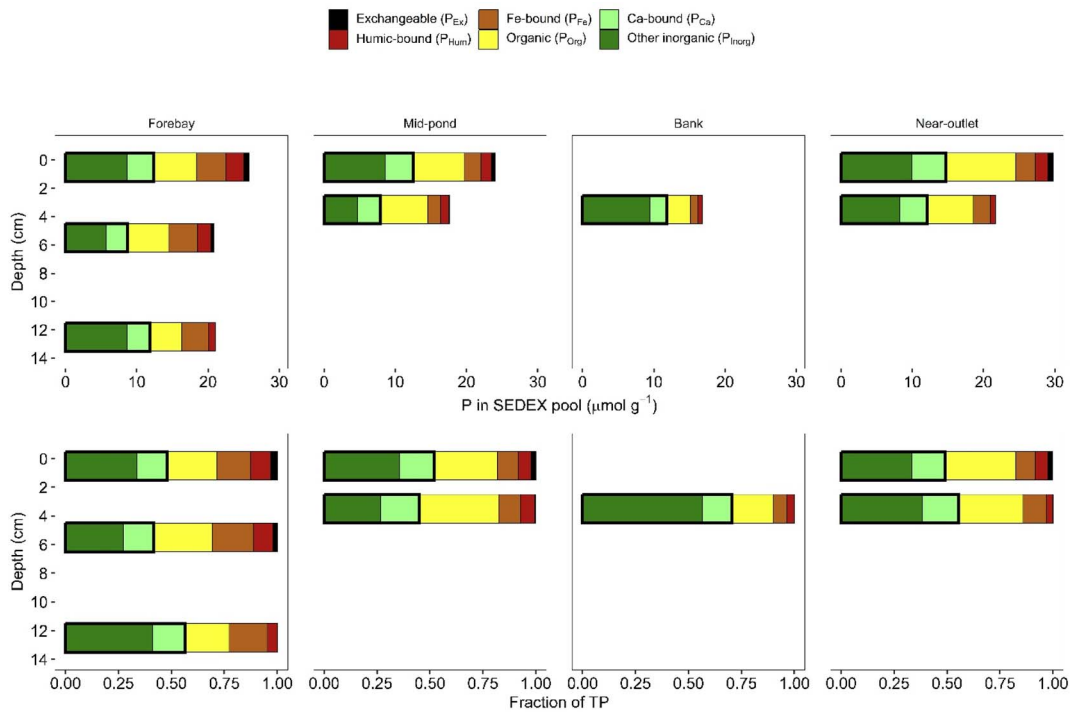

Fig. 5 Sediment phosphorus speciation: absolute values (top row) and relative concentrations (bottom row) of the P pools measured with the SEDEX sequential chemical extraction protocol as a function of depth in the sediment cores from the four different zones of the SWP (forebay, bank, mid-pond and near-outlet). From left to right, the SWP zones are ordered from closest to the inlet to closest to the outlet. The thick black outline shows the sum of the stable P pools.

sample had higher fractions of P_{Ex} (13%) and P_{Hum} (18%) compared to all other sediment samples on which SEDEX extractions were carried out. The Winter 2021 inlet and outlet suspended sediment samples had the third and second largest fractions of P_{Ex} (6% and 9%, respectively) of all the sediment samples extracted. We stress that the data on P concentration

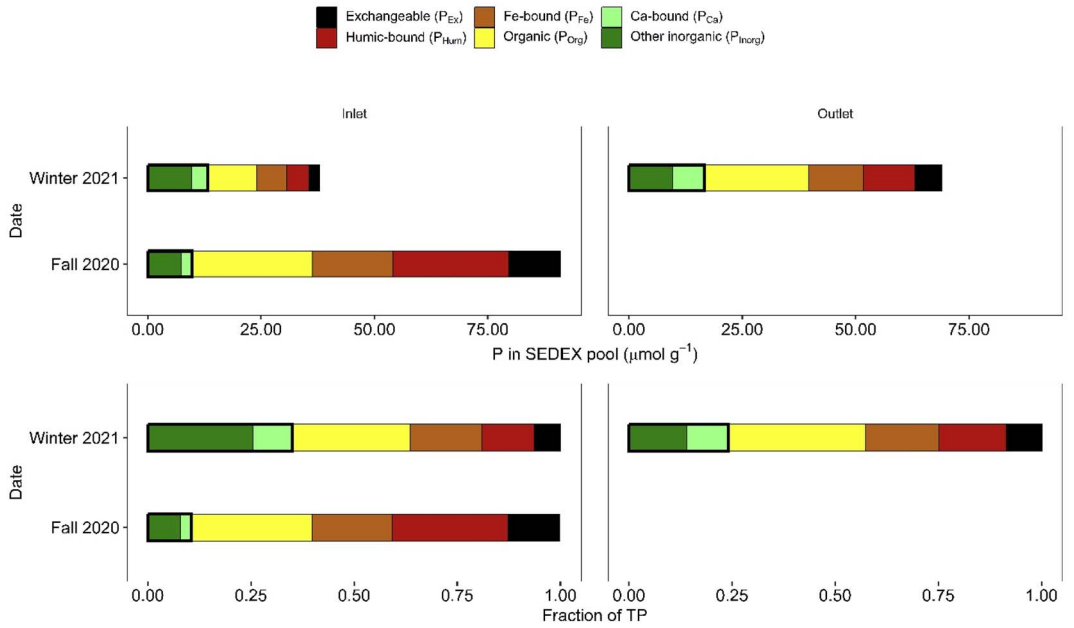

Fig. 6 Suspended matter phosphorus speciation: absolute (top row) and relative concentrations (bottom row) of the P pools measured with the SEDEX sequential chemical extraction protocol in stormwater suspended sediment samples collected at the pond inlet and outlet. Sampling season and year are noted on the *y*-axis. The thick black outline shows the sum of the stable P pools.

and speciation of the suspended sediments are preliminary because of the limited number and temporal coverage of the samples, as well as potential biases associated with the suspended sediment sampling methods used (ISCO samplers and continuous flow centrifuge, section 2.2.2).

3.4 Water column chemistry

The water column pH ranged between 7.3 and 9.5 with an average of 8.0 (Fig. S6a†), the DIC concentration ranged from 0.9 to 4.1 mmol L^{-1} with a mean of 2.4 mmol L^{-1} (Fig. S6b†), the dissolved Ca concentration ranged from 0.7 to 2.3 mmol L^{-1} with a mean of 1.4 mmol L^{-1} (Fig. S6c†). The DRP concentration ranged from 0.03 to 1.23 μmol L^{-1} with a mean of 0.27 μmol L^{-1} (Fig. S6d†). The pH was highest in the summer and dropped in fall and winter, whereas DCa and DIC followed opposite trends, reaching their lowest concentrations in summer (Fig. S6†). The concentrations of DIC and DCa closely correlated with a positive linear slope of 1.8 (Fig. S6†).

The summer and winter temperature profiles showed relatively gentle depth gradients (Fig. S7†). The mean water temperature (below the ice) in the winter profile was 4 °C. In the summer the surface water temperature reached 22 °C. The specific conductivity values in winter were higher than in summer with both profiles showing fairly steep gradients. In winter, the specific conductivity gradually increased from ~3000 to ~6000 μS cm^{-1} with increasing depth. In summer, the specific conductivity remained fairly constant between 0 and 0.9 m below the water surface, beyond which it increased from 2000 to 3800 μS cm^{-1} between 0.9 and 1.3 m and then stayed around 3800 μS cm^{-1} until the SWI at around 1.5 m below the water surface.

The pond water was supersaturated with respect to hydroxyapatite (HAP) and calcite in 90 and 63% of the collected samples, respectively (Fig. S8†). The pond water was undersaturated with respect to other more soluble calcium phosphate minerals, as well as non-calcium phosphate minerals such as strengite, vivianite and $MnHPO_4$.

4 Discussion

4.1 Dissolved P retention by mineral formation

The material fluxes, P speciation data, and gap-filling modeling, yields the annual mass balances for TP and constituent P pools shown in Fig. 3. Around 62% of the TP entering the SWP is estimated to be retained. In the conventional view that most TP retention is due to the trapping of P associated with suspended matter, the retention should be more efficient for PP than for dissolved forms of P. Our results, however, show exactly the opposite: the retention efficiencies of TDP (67%) and especially of DRP (81%) are much higher than that of PP (53%). Thus, processes other than just physical removal by sedimentation must control the removal of DRP in the SWP. The estimated TP removal efficiency by the SWP (62%) is close to median values reported for other sites in Ontario (see Table 3 of a report prepared by Hutchinson Consulting which reports TP removal efficiencies for other SWPs[40]), whereas the TDP and DRP reduction efficiencies are at the higher end for our site. With these high retention efficiencies, the SWP studied here falls in the 'enhanced protection' category of stormwater ponds according to the water quality objectives of the Ontario Ministry of Environment, Conservation and Parks.[41]

Changes in urban runoff loads of nutrient and other contaminants by SWPs depend on many factors, among others, inflow loads, pond size, water storage capacity, flow length, and maintenance regime.[42–44] The retention efficiency of P in reservoir-type systems has further been shown to correlate positively with the hydraulic residence time.[45] With increasing hydraulic residence time, the extent to which biogeochemical processes can transform the speciation of P and other nutrients and modulate their retention also increases.[46,47]

Here, we posit that biogeochemical reaction processes result in the transformation of DRP into stable phosphate-containing mineral phases that accumulate in the SWP's sediments. This first requires the transfer of DRP entering the SWP from the water column to the sediments. Likely pathways include uptake of DRP by algae and aquatic plants during photosynthesis and, potentially, DRP sorption to suspended matter, followed by deposition at the SWI. Such a scenario is in line with the chemical profiles measured in the sediment cores.

The near-constant TP concentrations with depth in the sediment cores (Fig. 4), coupled with the replacement of the most reactive P pools (P_{Ex}, P_{Hum} and P_{Org}) in the topmost sediments to more stable (less reactive) mineral P pools (P_{Ca} and P_{Inorg}) with increasing depth (Fig. 5 and S4†), points to a redistribution of P within the sediments. That is, mineralization of P-containing organic compounds, desorption from exchange sites, and degradation of ternary P complexes with humic substances[49] release dissolved phosphate ions that subsequently (co-)precipitate with mineral phases actively forming in the sediments.[14,49,50] The decreasing TOC concentrations with depth in the sediment cores (Fig. 4b) further support mineralization of labile organic matter as a major source of dissolved phosphate to the sediment pore water.[14] The positive correlation ($p < 0.05$) between the sum of the concentrations of the reactive P pools and the TOC concentration in the four cores (Fig. S9†) is consistent with the continuous transformation of reactive P forms to more stable ones with increasing depth in the sediments while, at the same time, organic matter is being degraded.

Post-depositional P redistribution leading to P incorporation into *in situ* forming (*i.e.*, authigenic) redox-stable mineral phases is also known as "sink-switching".[51,52] We propose that such sink-switching explains the very high retention (81%) of DRP in the Richmond Hill SWP. A key factor enabling this large role of mineral formation is the pond's water chemistry. The near-ubiquitous supersaturation with respect to hydroxyapatite observed in the water column is likely even more pronounced in the sediment because of the porewater build-up of dissolved phosphate typically observed right below the SWI.[53–55] The XRD analyses further reveal the abundant presence of calcite in the SWP's sediments (Table S2†), while the linear correlation between DIC and DCa (Fig. S10†) implies a major control on the SWP's water chemistry by calcite dissolution-precipitation.[56] Although calcite's sorption capacity for phosphate ions is in itself relatively low,[57,58] DRP adsorption to calcite can help initiate Ca phosphate mineral formation.[59,60]

The formation of P-containing Ca minerals (P–Ca) has previously been reported for urban streams and stormwater systems.[61] The consensus is that the formation of these mineral phases is promoted by moderately alkaline pH and elevated DCa and DRP concentrations, together with sufficiently long contact times.[62] The Richmond Hill SWP is located in a glacial till region where alkaline Ca-bicarbonate type waters are prevalent, hence creating favourable geochemical conditions for P–Ca mineral formation as inferred here for the SWP.[63,64]

The proposed immobilization of P by Ca minerals, *via* sorption and (co-)precipitation processes, provides a logical explanation of the results of the sequential chemical extraction data and it is supported by the complementary water chemical analyses. Potential Ca phosphate minerals, however, could not be directly detected by XRD analysis. This is not unexpected given that: (1) newly formed authigenic phosphate minerals are usually poorly crystalline,[49] and (2) the expected mineral abundances would be very low and difficult to detect by XRD even if the minerals were all crystalline. Assigning the formula weight of HAP ($Ca_5(PO_4)_3(OH)$: 502.3 g mol^{-1}) to the sum of P_{Ca} plus P_{Inorg} in the deeper core sections, the authigenic P mineral abundance would be at most 0.2 wt%. More advanced fingerprinting techniques will be needed to determine the exact nature of the mineral phases sequestering P in the SWP sediments.[65]

4.2 Seasonality in P export

Summer represents the major TP export season, mainly because most of the annual flow in and out of the SWP occurs during summer (Fig. S1†). Furthermore, in summer excess DUP is exported from the SWP: summer accounts for 55% of the annual DUP export but only 30% of DUP input (black bars in Fig. 2b). A possible explanation lies with the inclusion of dissolved organic P compounds in the operationally defined DUP pool (DUP = TDP – DRP). Assays conducted by Frost *et al.*[12] showed a release of dissolved organic P from urban pond sediments. Such a release is probable given the relatively high abundance of organic matter in urban SWPs.[16] Because these dissolved organic compounds can potentially be degraded enzymatically to DRP,[23] water quality implications of DUP export from stormwater ponds, especially in summer, will require further investigation.

Due to a malfunctioning of measuring equipment, we were unable to collect data for spring and early summer, a period of the year known to represent an important time window for P transport in urban residential watersheds.[66,67] During this period, TP and PP can be elevated due to litter decomposition over winter, new litter from leaf-out, and soil erosion prior to grass establishment. Our results may, therefore, not fully capture the seasonality of P retention. Nonetheless, on a yearly basis, the available water and sediment data support the crucial role played by mineral formation in the retention of P by the pond.

4.3 Internal P loading

Internal P loading, that is, the efflux of DRP from bottom sediments back into the water column is usually assumed to be coupled to the iron redox cycle.[68] When the bottom waters are oxygenated, ferric iron (Fe(III)) oxyhydroxides accumulating at

the SWI efficiently sorb dissolved phosphate ions, hence, preventing their efflux out of the sediment. Conversely, when the water overlying the sediment is anoxic, Fe(III) oxyhydroxides reductively dissolve and pore water dissolved phosphate ions are able to escape to the water column.

All indications are that the SWP sediments are highly reducing. This includes the systematic detection of framboidal pyrite (Fig. S4†) and siderite (Table S2†), as well as the sulfidic ("rotten egg") smell when the cores where retrieved. These observations are consistent with active Fe(III) and sulfate reduction activity.[69,70] The conductivity–depth profile observed in the summer (Fig. S7†) further shows that the water column periodically stratifies, which would restrict the downward diffusion of dissolved oxygen into the bottom water. As observed for other SWPs,[71,72] this likely leads to oxygen-free waters overlying the sediments.

At first sight, and in line with previous SWP studies,[16,17] the redox conditions would appear to favor DRP recycling from the sediments. In fact, internal loading explains why the outflow from some SWPs is enriched in DRP relative to the inflow.[73] The Richmond Hill SWP, however, exhibits the opposite behavior. That is, despite reducing conditions at the SWI, the proposed sink-switching from more reactive P pools into a stable (non-redox) mineral pool counteracts internal P loading and, hence, results in the net removal of DRP from the water column. A minor role of iron redox cycling in modulating P exchanges across the SWI may be due to the sequestration of iron in its ferrous form by pyrite and siderite (Table S2†). Overall, the Richmond Hill SWP greatly reduces the downstream transfer of DRP. Given that DRP is the most bioavailable form of P, SWPs that function similarly to the Richmond Hill SWP represent an effective green infrastructure option to protect receiving water bodies from cultural eutrophication.

4.4 Implications for P abatement

We attribute the excellent DRP retention performance of the Richmond Hill SWP to the moderately alkaline pH and elevated dissolved Ca concentrations of the inflowing urban runoff, plus the existence of a permanent water pool that provides enough time for the biogeochemical processing of incoming P. Where such conditions do not exist, a possible management option may be "liming", that is supplying amendments of basic Ca-rich materials, such as calcinated eggshells, spent lime, or steel slag. Liming has been successful in removing dissolved phosphate in experimental column systems[74] and in batch studies with wastewater[75] and simulated stormwater.[76] It has also been applied in field-scale treatments of stormwater[77] and agricultural runoff.[78] The use of Fe-containing materials to enhance DRP retention has also been considered,[76] but the immobilized P tends to be incorporated in Fe(III) oxyhydroxides that are not stable under reducing conditions.[68]

5 Conclusions

We developed a P mass balance for the Richmond Hill SWP utilizing data obtained from a combination of fieldwork, lab analyses, and modeling. Inflow and outflow discharge rates were measured, and gap-filled using statistical modeling. Water samples were analyzed in the lab and the results, together with the discharge data, enabled us to quantify annual loadings of P entering and leaving the SWP. We also took sediment cores and performed sequential chemical extractions to unravel the fate of P deposited at the SWI. The results highlight the important, yet often underappreciated, role of P sequestration into actively forming redox-stable minerals that accumulate in the bottom sediments. This P retention pathway is particularly crucial for reducing urban stormwater DRP loading and therefore protecting downstream P-limited aquatic ecosystems from eutrophication. We anticipate that further mass balance studies that account for the changes in chemical P speciation may help explain why some SWPs exhibit DRP retention and others DRP enrichment. The mechanistic and quantitative information derived from integrated approaches such as that presented here can inform the design and implementation of mitigation strategies that optimize the water quality benefits of stormwater management systems.

Data availability

The sediment core, suspended sediment chemistry and water column chemistry (including calculation of mineral saturation indices) data obtained in this study are openly available on the Federated Research Data Repository (FRDR) website at the following DOI: **https://doi.org/10.20383/103.0658**. The P species concentrations measured in the SWP inlet and outlet samples are openly available on the DataStream repository at the following DOI: **https://doi.org/10.25976/nwln-l648**.[39]

Conflicts of interest

There are no conflicts to declare.

Acknowledgements

This research was supported by the Natural Science and Engineering Research Council of Canada (NSERC) (Strategic Partnerships Grant STPGP-521515-18), and the Global Water Futures (GWF) program funded by the Canada First Research Excellence Fund (CFREF). We are grateful to the City of Richmond Hill and the Toronto and Region Conservation Authority (TRCA) for assisting with the data collection. We thank Marianne VanderGriendt, Shuhuan Li, Danielle Green, Maitri Lad, Nina Sattolo, Tara Ferguson, and Sam Smith for careful lab analyses, as well as Bowen Zhou, Ari Lisogorsky, and Jovana Radosavljevic for their help in collecting and sectioning the sediment cores, and Sarah Kaykhosravi for her support in the analysis of hydrological data.

References

1 W. W. Walker, Phosphorus removal by urban runoff detention basins, *Lake Reservoir Manage.*, 1987, **3**, 314–326.

2 V. Taguchi, T. Olsen, B. D. Janke, H. Stefan, J. Findlay and J. Gulliver, in *Stormwater Research Priorities and Pond Maintenance, Final Report*, Minnesota Pollution Control Agency, St. Paul, MN, 2018.
3 J.-P. Jenny, A. Normandeau, P. Francus, Z. E. Taranu, I. Gregory-Eaves, F. Lapointe, J. Jautzy, A. E. K. Ojala, J.-M. Dorioz, A. Schimmelmann and B. Zolitschka, Urban point sources of nutrients were the leading cause for the historical spread of hypoxia across European lakes, *Proc. Natl. Acad. Sci. U. S. A.*, 2016, **113**, 12655–12660.
4 D. W. Schindler, S. R. Carpenter, S. C. Chapra, R. E. Hecky and D. M. Orihel, Reducing phosphorus to curb lake eutrophication is a success, *Environ. Sci. Technol.*, 2016, **50**, 8923–8929.
5 J. C. Makarewicz, T. W. Lewis, I. Bosch, M. R. Noll, N. Herendeen, R. D. Simon, J. Zollweg and A. Vodacek, The impact of agricultural best management practices on downstream systems: soil loss and nutrient chemistry and flux to Conesus Lake, New York, USA, *J. Great Lakes Res.*, 2009, **35**, 23–36.
6 H. W. Goh, K. S. Lem, N. A. Azizan, C. K. Chang, A. Talei, C. S. Leow and N. A. Zakaria, A review of bioretention components and nutrient removal under different climates—future directions for tropics, *Environ. Sci. Pollut. Res.*, 2019, **26**, 14904–14919.
7 J. Liu and A. P. Davis, Phosphorus speciation and treatment using enhanced phosphorus removal bioretention, *Environ. Sci. Technol.*, 2014, **48**, 607–614.
8 M. O'Shea, M. Borst and C. Nietch, *The Role of Stormwater BMPs in Mitigating the Effects of Nutrient Overenrichment in the Urban Watershed*, 2012, pp. 1–16.
9 A. S. Chiandet and M. A. Xenopoulos, Landscape and morphometric controls on water quality in stormwater management ponds, *Urban Ecosyst.*, 2016, **19**, 1645–1663.
10 J. M. Hathaway, R. S. Tucker, J. M. Spooner and W. F. Hunt, A traditional analysis of the first flush effect for nutrients in stormwater runoff from two small urban catchments, *Water, Air, Soil Pollut.*, 2012, **223**, 5903–5915.
11 J. Vaze and F. H. S. Chiew, Nutrient loads associated with different sediment sizes in urban stormwater and surface pollutants, *J. Environ. Eng. (N. Y.)*, 2004, **130**, 391–396.
12 P. C. Frost, C. Prater, A. B. Scott, K. Song and M. A. Xenopoulos, Mobility and bioavailability of sediment phosphorus in urban stormwater ponds, *Water Resour. Res.*, 2019, **55**, 3680–3688.
13 D. D. Olding, T. S. Steele and J. C. Nemeth, Operational monitoring of urban stormwater management facilities and receiving subwatersheds in Richmond Hill, Ontario, *Water Qual. Res. J. Can.*, 2004, **39**, 392–405.
14 I. Markelov, R.-M. Couture, R. Fischer, S. Haande and P. Van Cappellen, Coupling water column and sediment biogeochemical dynamics: modeling internal phosphorus loading, climate change responses, and mitigation measures in Lake Vansjø, Norway, *J. Geophys. Res.: Biogeosci.*, 2019, **124**, 3847–3866.
15 C. T. Parsons, F. Rezanezhad, D. W. O'Connell and P. V. Cappellen, Sediment phosphorus speciation and mobility under dynamic redox conditions, *Biogeosciences*, 2017, **14**, 3585–3602.
16 K. Song, C. Winters, M. A. Xenopoulos, J. Marsalek and P. C. Frost, Phosphorus cycling in urban aquatic ecosystems: connecting biological processes and water chemistry to sediment P fractions in urban stormwater management ponds, *Biogeochemistry*, 2017, **132**, 203–212.
17 V. J. Taguchi, T. A. Olsen, P. Natarajan, B. D. Janke, J. S. Gulliver, J. C. Finlay and H. G. Stefan, Internal loading in stormwater ponds as a phosphorus source to downstream waters, *Limnol. Oceanogr. Lett.*, 2020, **5**, 322–330.
18 D. W. Price, J. M. Plach, H. P. Jarvie and M. L. Macrae, Contribution of bunker silo effluent discharged *via* a riparian zone to watershed phosphorus loads, *J. Great Lakes Res.*, 2021, **47**, 1296–1304.
19 J. Murphy and J. P. Riley, A modified single solution method for the determination of phosphate in natural waters, *Anal. Chim. Acta*, 1962, **27**, 31–36.
20 S. Ringuet, L. Sassano and Z. I. Johnson, A suite of microplate reader-based colorimetric methods to quantify ammonium, nitrate, orthophosphate and silicate concentrations for aquatic nutrient monitoring, *J. Environ. Monit.*, 2011, **13**, 370–376.
21 E. A. Dayton, S. Whitacre and C. Holloman, Comparison of three persulfate digestion methods for total phosphorus analysis and estimation of suspended sediments, *Appl. Geochem.*, 2017, **78**, 357–362.
22 N. Kao, M. Mohamed, R. J. Sorichetti, A. Niederkorn, P. V. Cappellen and C. T. Parsons, Phosphorus retention and transformation in a dammed reservoir of the Thames River, Ontario: Impacts on phosphorus load and speciation, *J. Great Lakes Res.*, 2022, **48**, 84–96.
23 K. R. Reddy and R. D. DeLaune, *Biogeochemistry of Wetlands: Science and Applications*, CRC Press, Boca Raton, 2008.
24 K. I. Aspila, H. Agemian and A. S. Y. Chau, A semi-automated method for the determination of inorganic, organic and total phosphate in sediments, *Analyst*, 1976, **101**, 187–197.
25 K. C. Ruttenberg, Development of a sequential extraction method for different forms of phosphorus in marine sediments, *Limnol. Oceanogr.*, 1992, **37**, 1460–1482.
26 D. S. Baldwin, The phosphorus composition of a diverse series of Australian sediments, *Hydrobiologia*, 1996, **335**, 63–73.
27 D. W. O'Connell, N. Ansems, R. K. Kukkadapu, D. Jaisi, D. M. Orihel, B. J. Cade-Menun, Y. Hu, J. Wiklund, R. I. Hall, H. Chessell, T. Behrends and P. Van Cappellen, Changes in sedimentary phosphorus burial following artificial eutrophication of Lake 227, Experimental Lakes Area, Ontario, Canada, *J. Geophys. Res.: Biogeosci.*, 2020, **125**, e2020JG005713.
28 K. C. Ruttenberg, N. O. Ogawa, F. Tamburini, R. A. Briggs, N. D. Colasacco and E. Joyce, Improved, high-throughput approach for phosphorus speciation in natural sediments *via* the SEDEX sequential extraction method: SPExMan-SEDEX, *Limnol. Oceanogr.: Methods*, 2009, **7**, 319–333.

29 D. L. Parkhurst and C. A. J. Appelo, Description of input and examples for PHREEQC version 3—a computer program for speciation, batch-reaction, one-dimensional transport, and inverse geochemical calculations, *U.S. Geological Survey Techniques and Methods*, 2013, 6th edn, ch. A43, vol. 6, p. 497.
30 S. V. Dorozhkin, Calcium orthophosphates ($CaPO_4$): Occurrence and properties, *Morphologie*, 2017, **101**, 125–142.
31 S. Achleitner, M. Möderl and W. Rauch, CITY DRAIN © – An open source approach for simulation of integrated urban drainage systems, *Environ. Model. Softw.*, 2007, **22**, 1184–1195.
32 F. H. S. Chiew and T. A. McMahon, Modelling runoff and diffuse pollution loads in urban areas, *Water Sci. Technol.*, 1999, **39**, 241–248.
33 J. E. Nash and J. V. Sutcliffe, River flow forecasting through conceptual models part I — A discussion of principles, *J. Hydrol.*, 1970, **10**, 282–290.
34 S. S. Shapiro and M. B. Wilk, An analysis of variance test for normality (complete samples), *Biometrika*, 1965, **52**, 591–611.
35 T. S. Breusch and A. R. Pagan, A Simple Test for Heteroscedasticity and Random Coefficient Variation, *Econometrica*, 1979, **47**, 1287–1294.
36 L. J. Brown, V. Taleban, B. Gharabaghi and L. Weiss, Seasonal and spatial distribution patterns of atmospheric phosphorus deposition to Lake Simcoe, ON, *J. Great Lakes Res.*, 2011, **37**, 15–25.
37 J. G. Winter, M. C. Eimers, P. J. Dillon, L. D. Scott, W. A. Scheider and C. C. Willox, Phosphorus inputs to Lake Simcoe from 1990 to lake water quality, *J. Great Lakes Res.*, 2007, **33**, 381–396.
38 B. D. Janke, P. Natarajan, J. S. Gulliver and J. C. Finlay, *Stormwater Pond Maintenance, and Wetland Management for Phosphorous Retention*, Minnesota Department of Transportation, 2023.
39 S. Slowinski, J. Radosavljevic, A. Graham, I. Ippolito, K. Thomas, F. Rezanezhad, M. Shafii, C. T. Parsons, N. B. Basu, J. Wiklund, R. I. Hall and P. Van Cappellen, Contrasting impacts of agricultural intensification and urbanization on lake phosphorus cycling and implications for managing eutrophication, *J. Geophys. Res.: Biogeosci.*, 2023, **128**, e2023JG007558.
40 Hutchinson Consulting, Phosphorus budget tool in support of sustainable development for the Lake Simcoe watershed, *Technical report prepared for Ontario Ministry of Environment, Conservation, and Parks*, 2012.
41 Ontario Ministry of the Environment, *Stormwater Management Plan and SWMP Design*, 2001.
42 B. D. Janke, J. C. Finlay, V. J. Taguchi and J. S. Gulliver, Hydrologic processes regulate nutrient retention in stormwater detention ponds, *Sci. Total Environ.*, 2022, **823**, 153722.
43 M. J. Sønderup, S. Egemose, A. S. Hansen, A. Grudinina, M. H. Madsen and M. R. Flindt, Factors affecting retention of nutrients and organic matter in stormwater ponds, *Ecohydrology*, 2016, **9**, 796–806.
44 M. Nayeb Yazdi, D. J. Sample, D. Scott, X. Wang and M. Ketabchy, The effects of land use characteristics on urban stormwater quality and watershed pollutant loads, *Sci. Total Environ.*, 2021, **773**, 145358.
45 T. Maavara, C. T. Parsons, C. Ridenour, S. Stojanovic, H. H. Dürr, H. R. Powley and P. V. Cappellen, Global phosphorus retention by river damming, *Proc. Natl. Acad. Sci.*, 2015, **112**, 15603–15608.
46 P. Van Cappellen and T. Maavara, Rivers in the Anthropocene: Global scale modifications of riverine nutrient fluxes by damming, *Ecohydrol. Hydrobiol.*, 2016, **16**, 106–111.
47 T. Maavara, Z. Akbarzadeh and P. Van Cappellen, Global dam-driven changes to riverine N:P:Si ratios delivered to the Coastal ocean, *Geophys. Res. Lett.*, 2020, **47**, e2020GL088288.
48 Y. Audette, D. S. Smith, C. T. Parsons, W. Chen, F. Rezanezhad and P. Van Cappellen, Phosphorus binding to soil organic matter via ternary complexes with calcium, *Chemosphere*, 2020, **260**, 127624.
49 P. V. Cappellen and R. A. Berner, Fluorapatite crystal growth from modified seawater solutions, *Geochim. Cosmochim. Acta*, 1991, **55**, 1219–1234.
50 S. R. Joshi, R. K. Kukkadapu, D. J. Burdige, M. E. Bowden, D. L. Sparks and D. P. Jaisi, Organic matter remineralization predominates phosphorus cycling in the mid-Bay sediments in the Chesapeake Bay, *Environ. Sci. Technol.*, 2015, **49**, 5887–5896.
51 C. März, S. W. Poulton, T. Wagner, B. Schnetger and H.-J. Brumsack, Phosphorus burial and diagenesis in the central Bering Sea (Bowers Ridge, IODP Site U1341): Perspectives on the marine P cycle, *Chem. Geol.*, 2014, **363**, 270–282.
52 K. C. Ruttenberg and R. A. Berner, Authigenic apatite formation and burial in sediments from non-upwelling, continental margin environments, *Geochim. Cosmochim. Acta*, 1993, **57**, 991–1007.
53 C. Hensen, M. Zabel and H. N. Schulz, in *Marine Geochemistry*, ed. H. D. Schulz and M. Zabel, Springer, Berlin, Heidelberg, 2006, pp. 207–240.
54 J. M. Novak, K. C. Stone, A. A. Szogi, D. W. Watts and M. H. Johnson, Dissolved phosphorus retention and release from a coastal plain In-stream wetland, *J. Environ. Qual.*, 2004, **33**, 394–401.
55 M. Sondergaard, J. P. Jensen and E. Jeppesen, Role of sediment and internal loading of phosphorus in shallow lakes, *Hydrobiologia*, 2003, **506–509**, 135–145.
56 W. Stumm and J. J. Morgan, *Aquatic Chemistry: Chemical Equilibria and Rates in Natural Waters*, Wiley, New York, 3rd edn, 1996.
57 M. E. Hamad, D. L. Rimmer and J. K. Syers, Effect of iron oxide on phosphate sorption by calcite and calcareous soils, *J. Soil Sci.*, 1992, **43**, 273–281.
58 P. Van Cappellen, L. Charlet, W. Stumm and P. Wersin, A surface complexation model of the carbonate mineral-aqueous solution interface, *Geochim. Cosmochim. Acta*, 1993, **57**, 3505–3518.

59 K. R. Reddy, R. H. Kadlec, E. Flaig and P. M. Gale, Phosphorus retention in streams and wetlands: a review, *Crit. Rev. Environ. Sci. Technol.*, 1999, **29**, 83–146.
60 C. Ren, Y. Li, Q. Zhou and W. Li, Phosphate uptake by calcite: Constraints of concentration and pH on the formation of calcium phosphate precipitates, *Chem. Geol.*, 2021, **579**, 120365.
61 Y. Liu, J. Goor and C. E. Robinson, Behaviour of soluble reactive phosphorus within field-scale bioretention systems, *J. Hydrol.*, 2021, **601**, 126597.
62 O. A. Diaz, K. R. Reddy and P. A. Moore, Solubility of inorganic phosphorus in stream water as influenced by pH and calcium concentration, *Water Res.*, 1994, **28**, 1755–1763.
63 L. Dyke, *Regional Groundwater and Stream Chemistry Survey, Oak Ridges Moraine, Ontario*, Geological Survey of Canada Current Research, 1999, 111–121.
64 Environment Canada, *Water Quality Interpretive Report, No. 3, Ontario, 1967-1977, Inland Waters Directorate, Water Quality Branch*, Ottawa, Canada, 1979.
65 J. F. Oxmann, Technical Note: An X-ray absorption method for the identification of calcium phosphate species using peak-height ratios, *Biogeosciences*, 2014, **11**, 2169–2183.
66 A. R. Bratt, J. C. Finlay, S. E. Hobbie, B. D. Janke, A. C. Worm and K. L. Kemmitt, Contribution of leaf litter to nutrient export during winter months in an urban residential watershed, *Environ. Sci. Technol.*, 2017, **51**, 3138–3147.
67 W. R. Selbig, Evaluation of leaf removal as a means to reduce nutrient concentrations and loads in urban stormwater, *Sci. Total Environ.*, 2016, **571**, 124–133.
68 D. M. Orihel, H. M. Baulch, N. J. Casson, R. L. North, C. T. Parsons, D. C. M. Seckar and J. J. Venkiteswaran, Internal phosphorus loading in Canadian fresh waters: a critical review and data analysis, *Can. J. Fish. Aquat. Sci.*, 2017, **74**, 2005–2029.
69 A. N. Roychoudhury, J. E. Kostka and P. Van Cappellen, Pyritization: a palaeoenvironmental and redox proxy reevaluated, *Estuarine, Coastal Shelf Sci.*, 2003, **57**, 1183–1193.
70 R. T. Wilkin, H. L. Barnes and S. L. Brantley, The size distribution of framboidal pyrite in modern sediments: An indicator of redox conditions, *Geochim. Cosmochim. Acta*, 1996, **60**, 3897–3912.
71 S. S. Ahmed, M. R. Loewen, W. Zhang, T. R. Ghobrial, D. Z. Zhu, K. Mahmood and B. van Duin, Field observations of stratification in stormwater wet ponds, *J. Environ. Manage.*, 2022, **322**, 115988.
72 N. A. McEnroe, J. M. Buttle, J. Marsalek, F. R. Pick, M. A. Xenopoulos and P. C. Frost, Thermal and chemical stratification of urban ponds: Are they 'completely mixed reactors', *Urban Ecosyst.*, 2013, **16**, 327–339.
73 B. Zhou, M. Shafii, C. T. Parsons, E. Passeport, F. Rezanezhad, A. Lisogorsky and P. Van Cappellen, Modeling multi-year phosphorus dynamics in a bioretention cell: Phosphorus partitioning, accumulation, and export, *Sci. Total Environ.*, 2023, **876**, 162749.
74 L. E. Christianson, C. Lepine, P. L. Sibrell, C. Penn and S. T. Summerfelt, Denitrifying woodchip bioreactor and phosphorus filter pairing to minimize pollution swapping, *Water Res.*, 2017, **121**, 129–139.
75 H. Yin, M. Kong and C. Fan, Batch investigations on P immobilization from wastewaters and sediment using natural calcium rich sepiolite as a reactive material, *Water Res.*, 2013, **47**, 4247–4258.
76 G. Prabhukumar, G. S. Bhupal and K. R. Pagilla, Laboratory evaluation of sorptive filtration media mixtures for targeted pollutant removals from simulated stormwater, *Water Environ. Res.*, 2015, **87**, 789–795.
77 A. C. Kuster, K. M. Pilgrim, A. T. Kuster and B. J. Huser, Field application of spent lime water treatment residual for the removal of phosphorus and other pollutants in urban stormwater runoff, *Water*, 2022, **14**, 2135.
78 T. Kirkkala, A.-M. Ventelä and M. Tarvainen, Long-term field-scale experiment on using lime filters in an agricultural catchment, *J. Environ. Qual.*, 2012, **41**, 410–419.